Journal of Applied Polymer Science

Structural Variations and Morphological Features of Polyethylene/Carbon Black Conductive Composites After Processing in an Internal Mixer

Chien-Lin Huang,[1] Yu-Chen Chen,[2] Chi Wang,[2] Ching-Fang Tu,[3] Fu-Sen Liao[3]

[1]Department of Fiber and Composite Materials, Feng Chia University, Taichung 407, Taiwan, ROC
[2]Department of Chemical Engineering, National Cheng Kung University, Tainan 701, Taiwan, ROC
[3]Department of Chemical Engineering, China Steel Corporation, Kaohsiung, Taiwan, ROC
Correspondence to: C. Wang (E-mail: chiwang@mail.ncku.edu.tw)

ABSTRACT: Polyethylene (PE) composites filled with carbon black (CB) were prepared using an internal mixer. Several analytical techniques, including rheometry, gel permeation chromatography, electrical conductivity measurements, differential scanning calorimetry, wide-angle X-ray diffraction, and transmission electron microscopy (TEM), were used to reveal the structural variations, thermal degradation, morphological features, and crystallization of the PE/CB conductive composites. It was found that the PE polymer chains were degraded, forming long-chain branching structures after over 30 min of internal mixing. The electrical conduction of the PE/CB composites was determined by the filler content and distribution. The electrical percolation threshold of the PE/CB composites was determined to be between 20 and 30 wt %. The addition of CB had no significant influence on the crystallinity of the PE/CB composites. In contrast, the electron-beam radiation dose had a significant effect on crystallinity. TEM micrographs of the PE/CB composites exhibit a random four-phase morphology, including PE lamellae, PE amorphous, CB particles, and voids at the PE/CB interface.
 J. Appl. Polym. Sci. 130: 1038–1046, 2013

KEYWORDS: composites; morphology; polyolefins; rheology; structure–property relations

Received 13 September 2012; accepted 3 March 2013; published online 17 April 2013
DOI: 10.1002/app.39251

INTRODUCTION

Polyethylene (PE) is the most common thermoplastic polymer currently available. It is ubiquitous in consumer products, such as packaging, insulating, and cushioning materials. Adding carbon black (CB) to the insulating PE matrix usually produces a conducting CB network. These PE/CB polymer composites show promising applications in electrostatic discharge, electromagnetic interference shielding, and polymeric positive temperature coefficient devices. The most common industrial methods for producing PE/CB composites are internal mixing and extrusion. PE degradation during processing is a critical issue not only because of its scientific importance, but also for technical reasons. According to Hinsken et al.,[1] the degradation mechanisms of high-density PE (HDPE) are chain scission and chain branching. El'darov et al.[2] pointed out the effects of shear rate and temperature on PE degradation. Moreover, Pinheiro et al.[3,4] verified that the oxygen concentration during HDPE processing results in different levels of chain scission and chain branching.

The electrical conduction of PE/CB composites is determined by the filler content and distribution in these composites. Percolation scaling laws offer a theoretical basis for the properties of suspensions and composites containing impenetrable particles to characterize the dispersion state of fillers.[5–7] Two material properties are widely used in the application of percolation theory to describe the dispersion state of CB in the polymer matrix: the electrical conductivity (σ) and the dynamic elastic moduli. The conductive composites are formed from the network connection of the CB filler above the percolation threshold of CB.[8] Zhang et al.[9] studied the relationship between the behavior of the dispersed fillers and the dynamic modulus. According to Wu et al.,[10] the electrical and rheological percolation thresholds for PE/CB composites are similar.

When the electrons pass the insulating PE matrix between agglomeration structure of CB above the percolation threshold of CB, the ample heat generated by the resistance within the system might melt the crystalline phase. Thus, the volume of the PE matrix expands, and the gap between the CB aggregates increases during PE melting. When the system cools down, the composites return to their original morphology and function as a conductor again. This phenomenon is called the positive

temperature coefficient (PTC) effect,[11–13] which is a common phenomenon for PE/CB conductive composites. In some special cases, when the system temperature is increased, its resistivity decreases rapidly. This opposite situation is called the negative temperature coefficient (NTC) effect[14] because the PE melt flows and the CB forms a new uniform distribution.

The movement of PE melts at high temperature is reduced provided that electron-beam (e-beam) radiation is applied to cross-link the amorphous chains between the PE lamellar crystals. This method effectively diminishes the NTC effect.[15] Zheng et al.[16] investigated the relationship between the PTC/NTC transition and the dynamic rheological properties of the PE/CB conduction composites. Luo et al.[17] showed that the PTC intensity is enhanced with increasing PE crystallinity in the PE/CB system. Park et al.[18] studied the effects of crystallinity on e-beam-radiated PE/CB composites. For quenched/e-beam-radiated and annealed/e-beam-radiated composites, no significant differences in crystallinity and sample resistivity were observed. However, when the PE received different radiation doses, two typical chemical changes occurred in the inter-lamellar amorphous region, namely, main-chain scission and cross-linking.[19–23] The effect of the radiation dose on the PE polymer chains can be correlated with the viscoelastic behavior of the PE samples.

During the processing of a PTC device of PE/CB composite, the PE chains are affected by the high temperature, mechanical stress, and e-beam radiation. Moreover, the conductivity of the PE/CB composites is affected by the CB dispersion state. The rheological properties of composites offer a theoretical basis to accurately characterize the PE structure and CB dispersion. In this article, we have studied the degradation levels, long chain branching (LCB), cross-linking, and filler dispersion of PE/CB composites by using several analytical techniques. We reported the formation of LCB structures of PE chains after composite compounding in an internal mixer. In addition, the effects of the CB addition and e-beam radiation on the PE crystallization were investigated.

EXPERIMENTAL

Material and Processing

HDPE and CB were used as the matrix material and filler, respectively. The as-received PE pellets had a density of 0.953 g/cm^3 and a melt flow index of 0.95 g/10 min. CB, with a density of 1.9 g/cm^3, was used as the electrically conductive medium of the composites. The PE/CB composites with various CB weight percentages (ϕ_w) were prepared using a lab-scale mixer (Plasti-Corder PL2000, Brabender) with a 55 cm^3 mixing chamber and a pair of roller blades. For all of the prepared samples, the compounding temperature was set to 190°C, and the roller speed was 40 rpm. The blended compounds were then compression-molded at 190°C for 10 min and subsequently cooled to room temperature to obtain 1 mm thick samples for further investigation. Composites with a ϕ_w of 10–45% were prepared in this manner. In this study, a 90/10 sample designation indicates the matrix-to-filler weight ratio.

The radiation of the PE/CB composites was conducted with an e-beam accelerator in air. The electron energy was 1.8 MeV with a beam current of 6.4 mA. A conveyor system was used in transporting the PE/CB composites at a speed of 10 m/min to receive radiation gradually until the desired dose was attained. The samples were irradiated to a total dose ranging from 0.2 MGy to 0.5 MGy for further studies. A 90/10-0.2 sample designation indicates 90/10 composites with 0.2 MGy of radiation.

High Temperature Gel Permeation Chromatography (HTGPC)

The weight-average molecular weight (M_w) and polydispersity ($p = M_w/M_n$, where M_n is the number-average molecular weight) of the samples were determined by HTGPC. A Waters Alliance GPCV 2000 system equipped with a differential refractive index detector and three columns (Styragel HMW 6E, HT 4, and HT 3) was used at 140°C with 1,2,4-trichlorobenzene as the mobile fluid and eight monodisperse atactic polystyrene standards (1.48–1270 kg/mol) for calibration.

Rheological Measurements

The pressed sample was tested using a strain-controlled rheometer (ARES, TA Instrument). The sample was pre-conditioned, and the thermal equilibrium was validated. Prior to the measurements, strain sweeps were performed to determine the strain range available for linear viscoelasticity at given frequencies of 0.1 and 100 rad/s. All the rheological experiments were conducted at 190°C under a nitrogen atmosphere to prevent a thermal degradation. Using a parallel-plate configuration (diameter: 25 mm, gap setting: 1 mm), a dynamic oscillation in the linear viscoelastic region was applied. The frequency sweep mode was used to obtain the dynamic storage modulus (G'), dynamic loss modulus (G''), and phase angle [$\delta = \tan^{-1}(G''/G')$]. The applied frequencies varied between 0.02 and 100 rad/s.

Gel Content Measurements

Gel content measurements were performed on the irradiated PE samples to determine the percentage of insoluble PE samples. The samples were weighed and subjected to a continuous Soxhlet extraction with *p*-xylene for 2 days according to the ASTM D2765 standard. The residues were dried in a vacuum. The gel content was calculated as the ratio of the final weight of the sample to its initial weight (in percentage).

Electrical Conductivity Measurements

For the samples with a high σ ($>10^{-6}$ S cm^{-1}), the measurements were carried out using a Keithley 2400 SourceMeter. The standard four-probe technique was applied to reduce the contact resistance effects. A Keithley 6487 electrometer equipped with a Keithley 8009 resistivity fixture was used for the samples with a σ ($< 10^{-6}$ S cm^{-1}) following the ASTM D257 standard.

Wide-Angle X-Ray Diffraction (WAXD) and Differential Scanning Calorimetry (DSC) Measurements

The WAXD patterns were obtained using a Rigaku Dmax2000 X-ray diffractometer under Cu K_α radiation to characterize the crystal lattice of the samples. The crystallization and melting behavior of the PE/CB composites were investigated using a Perkin-Elmer DSC7 differential scanning calorimeter (DSC) under a nitrogen atmosphere. Prior to the measurements, indium and zinc standards were used to calibrate the enthalpies of fusion and melting temperatures. The samples were held at

200°C for 10 min, followed by cooling at a rate of 10°C/min to study the melt crystallization. Subsequent heating was performed at a rate of 10°C/min.

Transmission Electron Microscopy (TEM) Observations

Ultrathin films with a thickness of ~ 50 nm were observed by TEM. For the composite samples, the films were prepared by sectioning the bulk samples at room temperature using an Ultracut UCT (Leica) microtome. Staining of the ultrathin film was subsequently carried out using a ruthenium tetroxide (RuO_4) vapor at room temperature. For the neat PE samples, however, pre-staining by RuO_4 vapor for 10 min was required to enhance the film integrity prior to the sectioning. TEM micrographs were obtained using a JEM-2000FX instrument (Jeol) operated at 80 kV.

RESULTS AND DISCUSSION

In this study, PE and CB were mixed in an internal mixer to produce PE/CB conductive composites. However, when CB is present in the sample, it is difficult to accurately characterize the PE chain structures. Thus, the neat PE was melt-processed in the internal mixer under different durations without CB to characterize the structural changes in the PE chains during processing. This method clearly reveals the thermo-mechanical influence on polymer structural changes without fillers during processing. Torque and temperature data were collected at various mixing times during PE compounding. Figure 1(a) shows the PE compounding results. The temperature rose quickly to 199°C within the first 5 min of mixing and remained unchanged afterwards. According to Campanelli,[24] energy is exchanged with the wall and rotors of the internal mixer chamber to disperse and masticate the polymer. The temperature of the sample during mixing is higher than that of the set temperature. It is due to the friction between polymer chains. When all of the materials were placed in the chamber for compounding, a maximum torque was observed [Figure 1(a)].

The measured torque monotonically decreased with mixing time. For a mixing time of 10 min, the final torque was about 21.8 Nm. When the mixing time was increased to 30 min (or 50 min), a small peak in the torque was observed and the final torque was about 16.9 Nm (or 14.0 Nm). The instantaneous torque acting on the rotors is directly proportional to the melt viscosity during mixing time, while the melt viscosity is related to numerous variables, including the chamber geometry, rotor geometry, and materials. Therefore, HTGPC and rheometry can help explain the structural changes in the PE chains during processing.

Figure 1(b) shows the molecular weight distribution (MWD) curves of the PE after compounded in the mixer at 190°C for different durations. For the as-received PE, the obtained M_w and p were 275 kg/mol and 2.02, respectively. After compounding in an internal mixer for 30 min, the obtained M_w and p of PE-30 min were 85 kg/mol and 4.46, respectively. The corresponding values for PE-50 min were 68 kg/mol and 9.17, respectively. Samples of PE-50 min and PE-30 min exhibited significantly broader distributions than the neat PE. The average molecular weight of PE decreases with increasing mixing time.

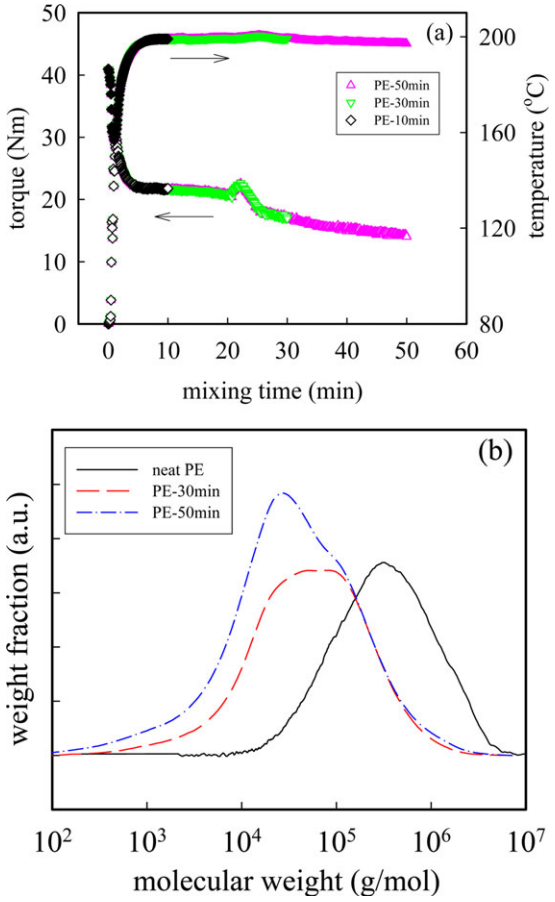

Figure 1. (a) Variation of mixing torques and temperatures of the PE during compounding in a Brabender internal mixer (open symbols for the measured torque and filled symbols for the measured temperature). (b) Molecular weight distribution of PE after compounding in the internal mixer for different periods. [Color figure can be viewed in the online issue, which is available at wileyonlinelibrary.com.]

The decrease in molecular weight is attributed to the thermo-mechanical degradation during mixing.[3] According to the literature,[2,4,25] chain scission and chain branching decrease the molecular weight. Oxygen concentration is an important consideration in thermo-mechanical degradation.[26–30] During internal mixing, polymer chains undergo scission because of the high temperature and large shear stress, thereby producing macroradicals. Under high oxygen concentration, polymer chains easily react with these macroradicals. Free radicals and unstable compounds form to attack the polymer chains, leading to increased degradation. However, when the oxygen content is low, these macroradicals react with one another, resulting in branching and unsaturated groups. Thus, PE degradation is an important phenomenon for PE/CB composites during compounding.

Rheological and Electrical Results

Prolonged measurement time on each testing sample was prevented, and a frequent validation of the data obtained was performed to ensure reproducibility. Figure 2(a) shows the G' and G'' of the PE samples processed in the internal mixer for different durations at 190°C. Compared with the modulus at a low

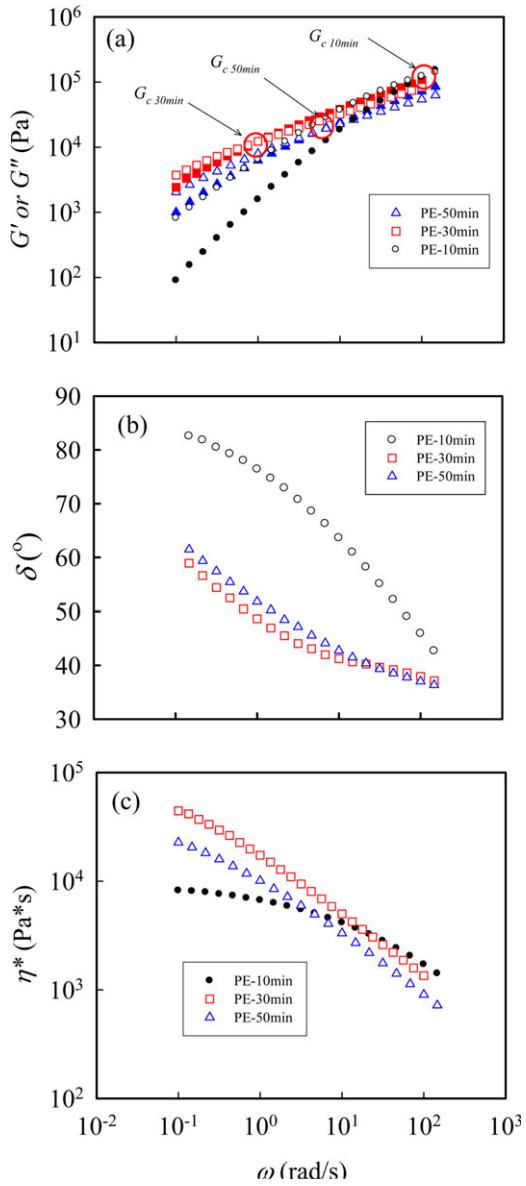

Figure 2. Comparison of the dynamic viscoelastic properties of PE-10min, PE-30min, and PE-50min at 190°C. (a) Storage modulus G' (filled symbols) and loss modulus G''(open symbols), (b) phase angle δ, and (c) complex viscosity η^*. [Color figure can be viewed in the online issue, which is available at wileyonlinelibrary.com.]

frequency, the G' of PE-30 min and PE-50 min were higher than that of PE-10 min. The G' of all the PE samples in the low-frequency region were lower than the corresponding G'', indicating a viscous dominance. When the frequency increases, the crossover point ($G' = G''$, G_c, and ω_c) appears, indicating an elastic dominance.

All of the materials have similar G' and G'' values in the high-frequency region. Moreover, the G' and G'' values of PE-30 min and PE-50 min are quite close. Based on the studies on the viscoelastic properties in the melt state,[31–33] G_c and ω_c are related to M_w, the degree of branching, and MWD. The G_c of PE-30 min and PE-50 min were 12,390 and 17,420 Pa, respectively. The ω_c of PE-30 min and PE-50 min were 1.0 and 5.4 rad/s, respectively. These G_c and ω_c values are significantly lower than those of PE-10 min, the G_c and ω_c of which were 128,000 Pa and 111.5 rad/s, respectively. The lower ω_c is possibly due to the increasing M_w or the branching structure of the PE material during processing. Based on the HTGPC results [Figure 1(b)], the increasing M_w is not possible. The lower G_c must be due to the wider MWD.

Figure 2(b) shows the variations in the phase angle (δ) versus the frequency of the PE samples, which is a sensitive property for LCB.[34–36] The δ is 90° in the low frequency region, provided that the liner polymer chain is completely relaxed. For the PE-10 min, the δ in the low-frequency region was 82.5°. At the given melting temperature of 190°C, several long chains were not completely relaxed for applied frequencies of 0.15 rad/s and above. However, for the PE-30 min and PE-50 min, a developing plateau was observed in the high-frequency region. The plateau for PE-30 min is slightly broader than that for PE-50 min. According to Wood-Adams et al.,[34] the δ behaviors of the branched polymer chains are significantly different. The LCB structure shows a plateau for the δ in the high-frequency region, and the plateau breadth increases with increasing LCB. Thus, the number of LCB chains of PE-30 min is greater than that of PE-50 min.

Viscosity is an important property in determining the processing feasibility of polymer melt. The complex viscosity (η^*) of the melt was derived from its dynamic properties (G' and G''). Figure 2(c) shows the derived η^* of the PE samples processed in the internal mixer for different durations at 190 °C. PE-10 min exhibited a Newtonian fluid behavior at low frequencies and became non-Newtonian at a ω higher than 0.32 rad/s. However, when the mixing time in the mixer was increased to 30 min, both the PE-30 min and PE-50 min melts exhibited a significant upturn in the flow curve in the low-frequency region. This increase is due to LCB structure formation. Moreover, the η^* of PE-30 min is higher than that of PE-50 min, suggesting that the M_w of PE-50 min is lower than that of PE-30 min. The trend is in good agreement with the HTGPC results [Figure 1(b)]. The degradation level for PE-50 min is higher than that for PE-30 min.

We believe that the formation of the LCB structures of the PE polymer chains is similar to that macroradicals, which form by thermo-mechanical stress, react with one another during mixing in the internal mixer. Based on the HTGPC and rheological experiment results, the PE polymer chains form numerous LCB structures at the peak in the torque at 22 min [Figure 1(a)]. To avoid branching structure formation during internal mixing and consequently affecting the processing characteristics of the composites, all the PE/CB samples were processed in the internal mixer for 10 min at 190°C.

Two typical relationships are expected from a homogeneous melt in the low-frequency region, that is, G'–$\omega^{2.0}$ and G''–$\omega^{1.0}$, provided the long chains are completely relaxed. For the PE melt at 190°C [Figures 3(a) and (b)], the exponents derived in the low-frequency region for G' and G'' were 1.70 and 0.96,

Applied Polymer SCIENCE

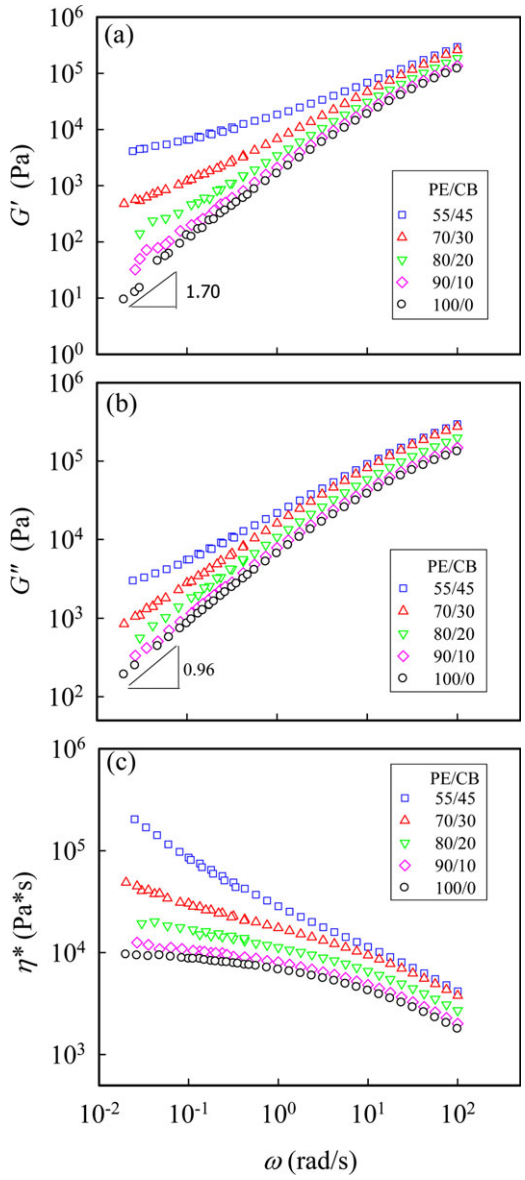

Figure 3. Comparison of the dynamic viscoelastic properties of the PE/CB composites at 190°C. (a) storage modulus G', (b) loss modulus G'' and (c) complex viscosity η^*. [Color figure can be viewed in the online issue, which is available at wileyonlinelibrary.com.]

respectively. The materials used for the PEs were commercial materials with relatively large MWDs [Figure 1(b)]. Given a melt temperature of 190°C, some long chains are not completely relaxed for an applied frequency of 0.02 rad/s, which is the lowest frequency applied in this study. When the applied frequency is lower than 0.02 rad/s, a longer time is required for data acquisition, thereby causing the thermal degradation of the melt.

Figure 3(a) shows the G' curves of the PE/CB melts obtained from the frequency sweep at 190°C. When the CB content was increased to 20 wt %, the slope in the low-frequency region decreased, and a small plateau was observed. However, no effect was observed in the high-frequency region. The plateau of the G' value increased with increasing CB content. A high CB loading eventually shifted the whole curve upward, and a significant filler effect on the chain dynamics was observed. With the increase in CB content to 45 wt %, the storage modulus at the low frequencies became less dependent on frequency, showing significant plateaus. These findings are in accordance with the results of previous studies, in which the formation of the interconnected CB structure is shown, leading to a percolation in an evident plateau for the storage modulus.[9,10]

Figure 3(b) shows the frequency dependency of G'' of the PE/CB melts at 190°C. Similar to the G' results, the slope in the low-frequency region gradually decreased with increasing CB content. The G'' increased with increasing CB content, and finally became independent of the applied frequency. However, at any given CB concentration, the increase in G' is more pronounced than the increase in G''.

Viscosity is an important property in determining the processing feasibility of composite melts. The melt viscosity is expected to increase with the addition of a filler. Furthermore, a high viscosity hinders the processability of the composites. Figure 3(c) shows the η^* behavior of the PE/CB composites at 190°C. Figure 3(c) also shows the results of the neat PE, in which a Newtonian flow behavior is exhibited at low frequencies and a non-Newtonian one at high frequencies. When the CB content increased to 10 wt %, the CB-filled melt showed a slight increase in η^* without clearly changing the curve shape. However, when the CB content increased to 30 wt %, the CB-filled melts exhibited a significant upturn in the flow curve in the low-frequency region. This yielding phenomenon typically indicates an elastic dominant behavior resulting from the formation of a sufficient CB network, which hinders the PE/CB composite melt flow.

Figure 4 shows the σ of the PE/CB composites as a function of filler content. For the neat PE, the measured σ was 1.97×10^{-18} S cm^{-1}. For the CB-filled samples, a mild increase in σ was observed with an increase in CB content to 20 wt %. Compared with the neat matrix, a 12-order increase in σ was observed for the PE/CB composites with a ϕ_w of 30 wt %. CB content of 45 wt % is required to achieve a σ of

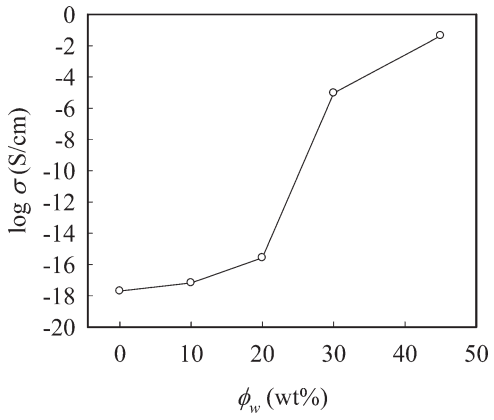

Figure 4. Electrical conductivity versus CB weight percentage of the PE/CB composites.

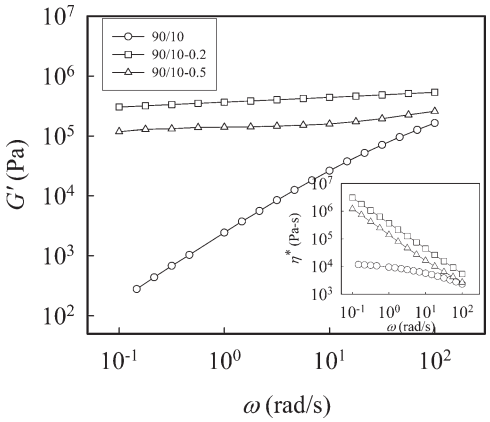

Figure 5. Effects of radiation dose on the dynamic storage modulus of the 90/10 composites as-revealed by the frequency sweep at 190°C. The inset shows the corresponding complex viscosity.

4.28×10^{-2} S cm^{-1}. The σ of the PE/CB composites suddenly increased when the CB content was varied from 20 to 30 wt %. The percolation scaling law can be applied in describing the relationship between σ and the percolation threshold. Thus, the law can determine quantitatively the minimum volume fraction of the fillers required to develop the filler network.[5–7] Whereas the σ data of the PE/CB composites are too limited with which to derive a precise percolation threshold, the electrical percolation threshold is roughly estimated to be 20–30 wt %. The addition of CB to PE also increases G'. Thus, the transition concentration is similar to that of the σ of the PE/CB composites.

Figure 5 shows the frequency dependence of G' curves of 90/10 composites irradiated at doses varying from 0.2 to 0.5 MGy at 190°C. By increasing the radiation dose to 0.2 MGy, the G' at low frequencies became independent of the applied frequency, forming a plateau. However, when the radiation dose increased to 0.5 MGy, the G' values of the 0.5 MGy composites were lower than that of the 0.2 MGy-treated composites. The exposure of the crystallized PE composites to radiation usually results in two typical chemical changes taking place in the interlamellar amorphous region. These chemical changes are main-chain scission and cross-linking. Therefore, the exposure of the PE/CB composites to low radiation doses causes a combination of chain scissioning and LCB. The exposure of the PE/CB composites to high radiation doses results in a cross-linking in the amorphous region of the PE.[21,23]

Based on our gel experiment, the PE gel content of composites subjected to 0.2 and 0.5 MGy radiation dose was 72 and 92%, respectively. The radiation doses are significant and slightly positively related to the PE chain cross-linking. A radiation dose of 0.2 MGy caused some LCB and cross-linking of the PE chain structure. Increasing the radiation dose to 0.5 MGy resulted in a further change of chain structure; the LCB content decreased and the cross-linking content increased. Therefore, the G' is lower as the 90/10 composites are subjected to a higher dose of e-beam. Thus, the number of LCB chains of 90/10-0.2 is greater than that of 90/10-0.5. This finding is in agreement with those of previous studies.[35,36] The effect of radiation dose on the complex viscosity of composites at 190°C is shown in the inset of Figure 5. With the presence of a small amount of LCB, the irradiated composites exhibit a dramatic increase in η^* and a typical behavior of non-Newtonian flow. It's of interest to note that η^* of the composites with 0.5 MGy radiation is lower than that with 0.2 MGy. According to García-Franco et al.,[35] PE with LCB shows physical gel-like behavior. Wood-Adams et al.[34] stated that the presence of LCB in PE chains added an additional long relaxation time. It indicates that the small amount of LCB structure enhances the G' and η^* of the partially cross-linked matrix.

WAXD and DSC Results

The WAXD intensity profiles and the index plane for each diffraction peak are shown in Figure 6. After the addition of CB (0–45 wt %), the PE/CB composites retained the neat PE crystals with an orthorhombic structure. When the 90/10 composites received various radiation doses (0–0.5 MGy), the composites exhibited the same neat PE crystals. No significant variation of WAXD profiles was observed in the irradiated composites, implying that the PE crystal lattices are radiation-stable up to 0.5 MGy.

To investigate melt crystallization, the composites were held at 200°C for 10 min, followed by cooling at a rate of 10°C/min. The DSC cooling curves are shown in Figure 7. The peak temperature and the integral area of the exotherm were determined and denoted by T_c and ΔH_c, respectively. ΔH_c is further normalized to the PE content to obtain $\Delta H'_c$ [$=\Delta H_c/(1 - \phi_w)$], which is used to represent the PE matrix crystallizability in the presence of CB. The data are listed in Table I. For the neat PE, T_c and $\Delta H'_c$ are 118.3°C and 191.1 J/g, respectively. With increasing CB content, a slight decrease in T_c is seen; being 116.6 and 116.1°C for the 90/10 and 55/45 composites. Regarding the $\Delta H'_c$, a more evident decrease is observed for the 90/10 composites. But, the filler effect becomes diminished for the 55/45 composite, exhibiting a $\Delta H'_c$ value of 181.3 J/g. These results indicate that the addition of CB marginally diminishes the crystallization rate of PE matrix, and the crystallizability of PE is slightly reduced.

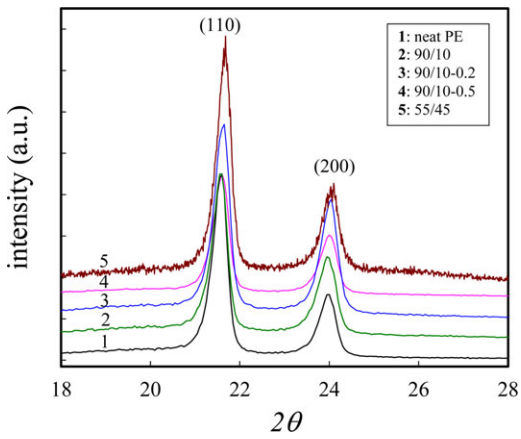

Figure 6. Effect of radiation dose on the WAXD intensity profiles of the PE/CB composites. [Color figure can be viewed in the online issue, which is available at wileyonlinelibrary.com.]

Applied Polymer SCIENCE

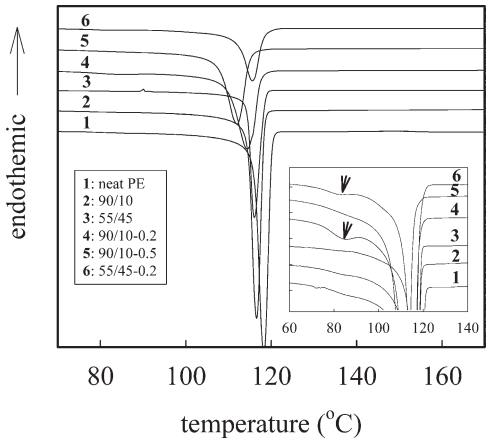

Figure 7. Cooling scans of PE/CB composites. The inset is the enlarged potion from 60 to 140°C. Prior to the cooling scan, the sample is held at 200°C for 10 min. Cooling rate: 10°C/min.

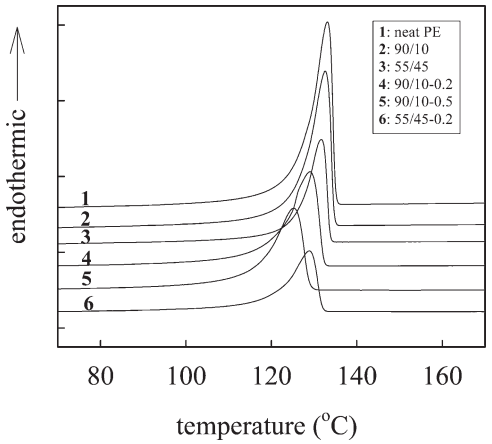

Figure 8. Melting behavior of the PE/CB composites after dynamic crystallization. Heating rate: 10°C/min.

After the composites are cooled to room temperature, the subsequent DSC heating curves are shown in Figure 8. The peak temperature and endothermic enthalpy were determined and denoted by T_m and ΔH_m, respectively. To compare the amount of melting crystals, ΔH_m was normalized to the PE content to derive the $\Delta H'_m$ [$=\Delta H_m/(1-\phi_w)$]. In addition, the crystalline fraction (ϕ^{DSC}) was calculated by the relation of $\Delta H'_m/\Delta H^o_m$, where $\Delta H^o_m = 280$ J/g is the melting enthalpy of the 100% pure PE crystals.[37] The derived results are listed in Table I as well. The neat PE showed a T_m of 133.1°C. After adding 10 wt % of CB, T_m became 132.6°C. Increasing the ϕ_w to 45 wt %, T_m slightly decreased to 131.6°C. It is well know that T_m is closely related to the lamellar thickness; the higher of the melting temperature, the thicker of PE lamellae developed in the composites. Therefore, the measured results of T_m imply that the thickness of PE lamellae is slightly reduced after the addition CB fillers. Regardless of the CB loading, the measured $\Delta H'_m$ is slightly larger than $\Delta H'_c$. It is attributed to the annealing effect during heating. For the neat PE, ΔH_m was 196.2 J/g, giving rise to a ϕ^{DSC} of 0.70. After adding CB fillers, ϕ^{DSC} was marginally reduced to 0.67 for the 90/10 composite, and to be 0.68 for the 55/45 composites. The effect of CB on the $\Delta H'_m$ showed results similar to those for the $\Delta H'_c$. In other words, the crystallizability of PE chains and the amount of lamellar crystals in the CB-filled composites slightly decreased with increasing filler content.

Table I. Thermal Properties of the PE/CB Composites Obtained by Dynamic Melt Crystallization

Sample code	T_c (°C)	$\Delta H'_c$ (J/g)	T_m (°C)	$\Delta H'_m$ (J/g)	ϕ^{DSC}
100/0	118.3	−191.1	133.1	196.2	0.70
90/10	116.6	−181.0	132.6	187.8	0.67
90/10-0.2	114.4	−162.7	129.0	151.6	0.54
90/10-0.5	112.1	−152.5	125.2	149.3	0.53
55/45	116.1	−181.3	131.6	191.1	0.68
55/45-0.2	115.6	−161.2	128.8	151.6	0.54

In the absence of e-beam radiation, the 90/10 composites showed a higher T_c than those under radiation. When the radiation was applied to a dose of 0.2 MGy, a barely discernible shoulder was seen at 85.5°C besides the apparent peak temperature at 114.4°C (Figure 7 inset). Subjected to the same radiation dose of 0.2 MGy, the 55/45-0.2 composite exhibits a similar crystallization shoulder at 85.5°C. However, at a higher radiation dose of 0.5 MGy, a single melt crystallization peak at 112.1°C was observed for the 90/10-0.5 composites. E-beam radiation frequently causes the branching and/or network microstructure of the PE chains, which further retards the melt crystallization. Thus, the slow kinetics occurring at the crystallization shoulder is attributed to the increased branching and/or network microstructure of the PE chains brought about by the radiation dose. Further increasing the radiation dose to 0.5 MGy led the LCB structure transferred into the cross-linking. Therefore, the disappearance of crystallization shoulder in the 90/10-0.5 composite is due to smaller ratio of LCB structure. The structural changes in the PE chains are in relatively good agreement with the rheological results of the e-beam radiation (Figure 5).

During the DSC heating trace, the T_m of 90/10-0.2 was suppressed and shifted to 129°C, as shown in Figure 8. By increasing the radiation dose to 0.5 MGy, the T_m decreased to 125.2°C. The e-beam radiation on the melt-crystallized sample effectively induced the cross-linking reaction of the amorphous chains between the lamellar crystallites. The radiation dose-dependence of T_m implies that higher doses lead to a slightly reduced lamellar thickness and/or to the destruction of the crystal structure.

The $\Delta H'_c$ was slightly larger than the $\Delta H'_m$ regardless of the radiation dose. The $\Delta H'_c$ of the 90/10 composites decreases with increasing radiation dose from 181.0 J/g, for the pristine composites, to 152.5 J/g, for those that received 0.5 MGy of radiation dose. A radiation dose effect was also observed. For the 90/10 composites, the $\Delta H'_m$ was 187.8 J/g. When the radiation dose was increased to 0.5 MGy, the measured and normalized $\Delta H'_m$ decreased to 149.3 J/g. Therefore, the ϕ^{DSC} became 0.67 for the 90/10 composites. After increasing the radiation dose to 0.5 MGy, the measured ϕ^{DSC} decreased to 0.53. The PE

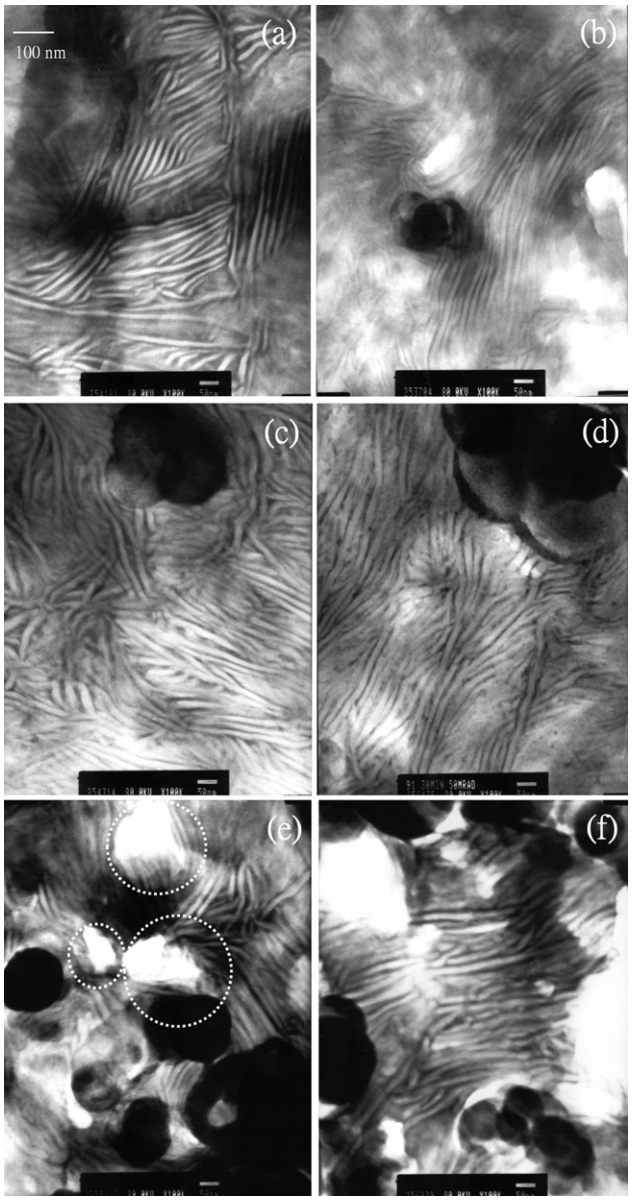

Figure 9. TEM micrographs of the PE/CB composites. (a) Neat PE, (b) 90/10, (c) 90/10-0.2, (d) 90/10-0.5, (e) 55/45, and (f) 55/45-0.2 The dashed circles indicate the empty spaces left behind after the extraction of the CB particles by sectioning.

chain crystallizability decreases with increasing radiation dose. When the radiation dose increases, a cross-linking reaction occurs. This reaction results in the branching and/or network microstructure of the PE chains, further retarding the dynamic crystallization.[20,38] Thus, the radiation doses have a significant effect on PE crystallinity.

TEM Results

Figure 9 shows several typical TEM micrographs. These images reveal the effects of the CB content and e-beam radiation on the composite morphology. The TEM micrographs show the edge-on PE lamellae as bright lines after the amorphous regions were preferentially stained with RuO_4 vapors, giving a relatively darkened appearance. Based on the TEM micrographs shown in Figures 9(b)–(d), the PE lamellae become more branched and randomly oriented after e-beam radiation. The crystalline lamellae thickness is indicated by the line width. Based on these micrographs, the average lamellar thickness, l_c, could be obtained from a collection of $\sim$ 300 lamellae. Regardless of the CB content and radiation dose, l_c remained unchanged (12–14 nm). TEM results are in conjunction with the corresponding melting temperatures determined by DSC heating scan. A variation in T_m was observed, but the effect of CB is marginal. However, the samples for the DSC measurements were held at 200°C for 10 min, followed by cooling at a rate of 10°C/min to study melt crystallization. The subsequent heating to 200°C was conducted at a rate of 10°C/min. In contrast, the samples for the TEM observation were not subjected to any heat treatment. For the TEM observation, after the composites received various radiation doses, the composites displayed the same PE lamellar thicknesses. Moreover, when the radiation composites melted by heating and then cooling them to room temperature, the PE lamellar thickness decreased.

Based on the TEM micrographs shown in Figures 9(b)–(f), the CB particles and aggregates have a larger mass density than the PE matrix. Therefore, the CB particles appeared to be much darker than the PE matrix. However, when the CB content increased, the TEM micrographs of the PE/CB composites exhibited a random four-phase morphology. PE lamellae, PE amorphous, CBs, and voids were clearly observed [Figure 9(e)]. The dashed circles indicate the empty spaces left behind after the CB particles extractions through cutting. These spaces further suggest the presence of voids at the PE/CB interface.

Marr et al.[39,40] presumed that a strong electron density contrast exists between the CB, PE, and voids, making the interpretation of scattering data highly complex. The authors, thus, used the unique capabilities of small-angle neutron scattering (SANS) to overcome these difficulties. SANS has a high bulk penetrating power and the ability to manipulate local scattering amplitudes via isotopic labeling (deuteration). Our TEM micrographs [Figures 9(e) and (f)] are good agreement with several studies.[39–41] The melt viscosity of the PE/CB composites increases during mixing because of the filler addition. The high viscosities of the PE/CB composites suggest that the CB network hinders the PE melt to flow into the small spaces between the CBs. Therefore, the voids formed in the composites.

Based on the TEM observations [Figures 9(b)–(f), the diameters of the primary CB particles were about 40–70 nm, but the sizes of the CB aggregates in the PE/CB composites were about 200–800 nm. When the CB content increased from 10 wt % to 45 wt %, the aggregate size increased, and the distance between the CB aggregates decreased. These results are in agreement with our conduction study. The shorter distance between the CB aggregates helps promote the electrical conduction of the network.

CONCLUSIONS

PE degradation is an important issue in the compounding of PE/CB composites using an internal mixer. The PE polymer

chains degraded, forming LCB structures during an internal mixing of over 30 min. The electrical percolation threshold of the PE/CB composites was determined to be between 20 wt % and 30 wt %. Adding CB slightly affected the PE/CB composite crystallinity. However, when the radiation dose was increased, cross-linking reactions took place, resulting in the branching and/or network microstructure of the PE chains and further retardation of the dynamic crystallization and crystallinity of the composites.

The presence of a small amount of LCB brought about by radiation affected the complex viscosity of composite melt. The complex viscosity of the PE composites exposed to 0.5 MGy radiation was lower than those exposed to 0.2 MGy radiation. Increasing the CB content from 10 to 45 wt % resulted in larger CB aggregates and decreased the distance between these aggregates. The addition of CB increased the CB phase domain and decreased the PE phase domain. The melt viscosity of the PE/CB composites increased with filler addition. The high viscosities of the PE/CB composites suggest that the CB network hinders the PE melt to flow into the small spaces between the CBs. The TEM micrographs of the PE/CB composites displayed a random four-phase morphology, including PE lamellae, PE amorphous, CBs, and voids

ACKNOWLEDGMENTS

The authors are grateful to the China Steel Corporation (Taiwan) for the research grant that supported this work.

REFERENCES

1. Hinsken, H.; Moss, S.; Pauquet, J. R.; Zweifel, H. *Polym. Degrad. Stab.* **1991**, *34*, 279.
2. El'darov, E. G.; Mamedov, F. V.; Goldberg, V. M.; Zaikov, G. E. *Polym. Degrad. Stab.* **1996**, *51*, 271.
3. Pinheiro, L. A.; Chinelatto, M. A.; Canevarolo, S. V. *Polym. Degrad. Stab.* **2006**, *91*, 2324.
4. Pinherio, L. A.; Chinelatto, M. A.; Canevarolo S. V. *Polym. Degrad. Stab.* **2004**, *86*, 445.
5. Bunde, A.; Havlin, S. Fractals and Disordered System, 2nd ed; Springer: New York, **1996**, 27.
6. Heaney, M. B. *Phys. Rev. B* **1995**, *52*, 12477.
7. Garboczi, E. J.; Snyder, K. A.; Douglas, J. F.; Thorpe, M. F. *Phys. Rev. E* **1995**, *52*, 819.
8. Liao, F. S.; Tu, C. F.; Lo, H. H.; Chu, C. F. *China Steel Technical Report* **2004**, *18*, 51.
9. Zhang, J. F.; Yi, X. S. *J. Appl. Polym. Sci.* **2002**, *86*, 3527.
10. Wu, G.; Zheng, Q. *J. Polym. Sci. Part B: Polym. Phys.* **2004**, *42*, 1199.
11. Tang, H.; Chen, X.; Luo, Y. *Eur. Polym. J.* **1997**, *33*, 1383.
12. Carmona, F. *Physica A* **1989**, *157*, 461.
13. Viswanathan, R.; Heaney, M. B. *Phys. Rev. Lett.* **1995**, *75*, 4433.
14. Nakis, M.; Ram, A.; Flashner, F. *Polym. Eng. Sci.* **1978**, *18*, 649.
15. Campanell, J. R.; Gurer, C.; Rose, T. L.; Varner, J. E. *Polym. Eng. Sci.* **2004**, *44*, 1247.
16. Zheng, Q.; Song, Y.; Wu, G.; Song, X. *J. Polym. Sci. Part B: Polym. Phys.* **2003**, *41*, 983.
17. Luo, Y.; Wang, G.; Zhang, B.; Zhang, Z. *Eur. Polym. J.* **1998**, *34*, 1221.
18. Park, E. S. *Macromol. Mater. Eng.* **2006**, *291*, 690.
19. Takashika, K.; Oshima, A.; Kuramoto, M.; Seguchi, T.; Tabata, Y. *Radiat. Phys. Chem.* **1999**, *55*, 399.
20. Lugão, A. B.; Hutuzler, B.; Ojeda, T.; Tokumoto, S.; Siemens, R.; Makuuchi, K.; Villavicencio, AL. C. H. *Radiat. Phys. Chem.* **2000**, *57*, 389.
21. Valenza, A.; Gallo, L.; Spadaro, G.; Calderadro, E. *Polym. Eng. Sci.* **1993**, *33*, 1336.
22. Birkinshaw, C.; Buggy, M. *J. Appl. Polym. Sci.* **1990**, *41*, 1913.
23. Chen, S.; Phillips, E.; Parks, L. *Radiat. Phys. Chem.* **2009**, *78*, 563.
24. Campanell, J. R.; Gurer, C.; Rose, T. L.; Varner, J. E. *Polym. Eng. Sci.* **2004**, *44*, 1247.
25. Kostadinova Loultcheva, M.; Proietto, M.; Jilov, N.; La Mantia, F. P. *Polym. Degrad. Stab.* **1997**, *57*, 77.
26. Holmström, A.; Sörvik, E. M. *J. Polym. Sci. Polym. Chem. Ed.* **1978**, *16*, 2555.
27. Rideal, G. R.; Padget, J. C. *J. Polym. Sci.: Polym. Symp.* **1976**, *57*, 1.
28. Gugumus, F. *Polym. Degrad. Stab.* **1995**, *49*, 29.
29. Gugumus, F. *Polym. Degrad. Stab.* **2000**, *68*, 21.
30. Gugumus, F. *Polym. Degrad. Stab.* **2000**, *69*, 29.
31. Yang, Q.; Chung, T. S.; Weber, M.; Wollny, K. *Polymer* **2009**, *50*, 524.
32. Yamaguchi, M.; Wanger, M. H. *Polymer* **2006**, *47*, 3629.
33. Cruz, S. A.; Zanin, M. *Polym. Degrad. Stab.* **2003**, *80*, 31.
34. Wood-Adams, P. M.; Dealy, M. J.; deGoot, A. W.; Redwine, O. D. *Macromolecules* **2000**, *33*, 7489.
35. García-Franco, C. A.; Srinivas, S.; Lohse, D. J.; Brant, P. *Macromolecules* **2001**, *34*, 3115.
36. Jørgensen, J. K.; Stori, A.; Redford, K.; Ommundsen, E. *Polymer* **2005**, *46*, 12256.
37. Chiang, R.; Flory, P. J. *J. Am. Chem. Soc.* **1961**, *83*, 2857.
38. Khonadkdar, H. A.; Jafari, S. H.; Wagenknecht, U.; Jennichen, D. *Radiat. Phys. Chem.* **2006**, *75*, 78.
39. Marr, D. W. M.; Wartenberg, M.; Schwartz, K. B.; Agamalian, M. M.; Wigmall, G. D. *Macromolecules* **1997**, *30*, 2120.
40. Marr, D. W. M.; Oakey, J.; Wartenberg, M.; Schwartz, K. B. *Macromolecules* **1999**, *32*, 5399.
41. Oakey, J.; Marr, D. W. M.; Schwartz, K. B.; Wartenberg, M. *Macromolecules* **2000**, *33*, 5198.